



Article

# Thermomechanical Responses and Energy Conversion Efficiency of a Hybrid Thermoelectric–Piezoelectric Layered Structure

Zhihe Jin <sup>1,\*</sup> and Jiashi Yang <sup>2,\*</sup>

<sup>1</sup> Department of Mechanical Engineering, University of Maine, Orono, ME 04469, USA

<sup>2</sup> Department of Mechanical and Materials Engineering, University of Nebraska, Lincoln, NE 68588, USA

\* Correspondence: zhihe.jin@maine.edu (Z.J.); jyang1@unl.edu (J.Y.)

**Abstract:** This paper develops a thermoelectric (TE)–piezoelectric (PE) hybrid structure with the PE layer acting as both a support membrane and a sensor for the TE film for microelectronics applications. The TE and PE layers are assumed to be perfectly bonded mechanically and thermally but electrically shielded and insulated with each other. The thermo-electro-mechanical responses of the hybrid bilayer under the TE generator operation conditions are obtained, and the influence of the PE layer on the TE energy conversion efficiency is investigated. The numerical results for a Bi<sub>2</sub>Te<sub>3</sub>/PZT-5H bilayer structure show that large compressive stresses develop in both the PE and TE layers. With a decrease in the PE layer thickness, the magnitude of the maximum compressive stress in the PE layer increases whereas the maximum magnitude of the stress in the TE layer decreases. The numerical result of the TE energy conversion efficiency shows that increasing the PE layer thickness leads to lower energy conversion efficiencies. A nearly 40% reduction in the peak efficiency is observed with a PE layer of the same thickness as that of the TE layer. These results suggest that design of TE films with supporting/sensing membranes must consider both aspects of energy conversion efficiency and the thermomechanical reliability of both the TE and PE layers.

**Keywords:** piezoelectricity; thermoelectricity; laminate; thermo-electro-mechanical responses; energy conversion efficiency



Citation: Jin, Z.; Yang, J.

Thermomechanical Responses and Energy Conversion Efficiency of a Hybrid Thermoelectric–Piezoelectric Layered Structure. *J. Compos. Sci.* **2024**, *8*, 171. <https://doi.org/10.3390/jcs8050171>

Academic Editor: Zhong Hu

Received: 6 March 2024

Revised: 14 April 2024

Accepted: 3 May 2024

Published: 6 May 2024



**Copyright:** © 2024 by the authors. Licensee MDPI, Basel, Switzerland. This article is an open access article distributed under the terms and conditions of the Creative Commons Attribution (CC BY) license (<https://creativecommons.org/licenses/by/4.0/>).

## 1. Introduction

Thermoelectric (TE) thin films have been developed for microelectronics applications; see for example, Rowe et al. [1], Volklein et al. [2], Venkatasubramanian et al. [3], Chen et al. [4], Kogo et al. [5], Corbett et al. [6], Nandihalli [7], and Mele et al. [8]. These TE films can be used to convert the waste heat (for example, the heat generated by the computer processors) into electric power. TE films have also been investigated to harvest human body heat in wearable electronics applications [8,9]. TE films when subjected to the temperature differential applied at the two ends of the film may be susceptible to mechanical instability due to their small thicknesses. Normally, TE films are deposited on a support membrane to increase its mechanical stability [2].

Thermal stresses in a TE film as well as in the supporting membrane are of importance in assessing the thermomechanical reliability of the TE device. Huang et al. [10,11] investigated the thermal stresses in a four-layer TE structure consisting of two TE films, a supporting layer and an insulation layer using both a one-dimensional (1D) analytical solution and a two-dimensional (2D) finite element method. Jin [12] calculated the thermal stresses in a four-layer TE structure using a laminated composites theory. Jin and Yang [13] analyzed a three-layer piezothermoelectric laminated structure consisting of an n-type piezothermoelectric film sandwiched between two support membranes. They considered the effects of carrier diffusion on the thermomechanical responses of the laminate.

In addition to the analytical and numerical solutions of the stress and deformation states in a TE structure that can be used to predict the mechanical failure, structural health

monitoring tools can also be used to evaluate the deformation and damage development in a TE structure. Piezoelectric sensors have widely been used to obtain the real-time information of the stress and deformation states in materials and structures [14–16]. Although both piezoelectric fibers and films may be used to detect damage development in engineering structures, piezoelectric membranes are a preferred geometrical configuration for monitoring TE films with microscopic thicknesses. Use of piezoelectric fibers and membranes, however, may negatively influence the energy conversion efficiency of the TE device. We point out that using piezoelectric sensors for structural health monitoring of TE devices has not been studied to the best knowledge of the authors.

This work aims to explore a concept of using a piezoelectric (PE) layer as both a supporting membrane and a sensing film. By replacing the regular support membrane for thin TE legs with a PE membrane, the structural health of the TE film can be monitored and the film can still maintain its mechanical stability. In the meantime, no additional energy conversion efficiency reduction will be incurred. We will analyze the thermo-electro-mechanical responses of the hybrid TE-PE layered structure and examine the effect of lamination on the TE energy conversion efficiency. The remainder of this paper is organized as follows. Section 2 presents the basic equations of thermoelectricity and piezoelectricity and the governing equations for the TE-PE laminate. The temperature, deformation, stress, and electric field in the TE-PE laminate are obtained in Sections 3 and 4, respectively. The equation to compute the energy conversion efficiency is presented in Section 5. In Section 6, numerical examples are presented for the temperature, deformation, stress, electric field, and energy conversion efficiency for a Bi<sub>2</sub>Te<sub>3</sub>/PZT-5H bilayer structure. Finally, conclusions are provided in Section 7.

## 2. Basic Equations

Consider a TE film deposited on a PE membrane as shown in Figure 1. The TE and PE layers have thicknesses  $t_1$  and  $t_2$ , respectively, and the length of the bilayer structure in the thermal gradient direction is denoted by  $L$ . The hybrid bilayer structure is mechanically fixed at the two ends and is subjected to a hot side temperature  $\Theta_h$  at  $z = L$  and cold side temperature  $\Theta_c$  at  $z = 0$ . We begin with the basic equations of thermoelectricity and piezoelectricity. The constitutive relations for isotropic thermoelectric materials are given by

$$\begin{aligned} J_i &= \sigma E_i - \sigma S \Theta_{,i} \\ h_i &= -k \Theta_{,i} + S \Theta J_i \\ T_{ij} &= 2GS_{ij} + \frac{2G\nu}{1-2\nu} S_{kk} \delta_{ij} - K\alpha(\Theta - \Theta_c) \delta_{ij} \end{aligned} \tag{1}$$

where  $\Theta$  is the temperature field,  $E_i$  is the electric field vector,  $J_i$  is the electric current density vector,  $h_i$  is the heat flux vector,  $T_{ij}$  is the stress tensor,  $S_{ij}$  is the strain tensor,  $\delta_{ij}$  is the Kronecker delta,  $\sigma$  is the electrical conductivity,  $S$  the Seebeck coefficient,  $k$  the thermal conductivity,  $G$  the shear modulus,  $\nu$  the Poisson’s ratio,  $\alpha$  the coefficient of thermal expansion, and  $K$  the bulk modulus. It is noted that  $S$  without the indices denotes the Seebeck coefficient but not the strain tensor.

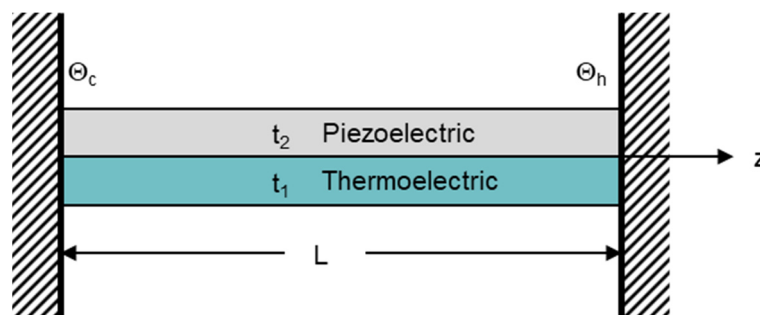


Figure 1. A thermoelectric-piezoelectric bilayer of length  $L$  subjected to a temperature differential.

The constitutive equations of piezoelectric materials are

$$\begin{aligned} T_{ij} &= c_{ijkl}S_{kl} - e_{kij}E_k - \lambda_{ij}(\Theta - \Theta_c) \\ D_i &= e_{ikl}S_{kl} + \varepsilon_{ik}E_k + p_i(\Theta - \Theta_c) \\ h_i &= -k_{ij}\Theta_{,j} \end{aligned} \tag{2}$$

where  $D_i$  is the electric displacement vector,  $k_{ij}$  the thermal conductivity tensor,  $c_{ijkl}$  the elastic stiffness,  $e_{ijk}$  the piezoelectric constants,  $\varepsilon_{ij}$  the dielectric constants,  $\lambda_{ij}$  the stress-temperature coefficients, and  $p_i$  the pyroelectric constants. In the above equations, the indices  $i, j, k, l$  have the range of 1 to 3, repeated indices imply summation over the range of the index, and a comma followed by index  $i$  implies partial derivative with respect to coordinate  $x_i$ .

The energy and charge balance equations in thermoelectricity under steady state conditions include

$$\begin{aligned} h_{i,i} &= J_j E_j \\ J_{i,i} &= 0 \end{aligned} \tag{3}$$

The charge equation of electrostatics of piezoelectricity is

$$D_{i,i} = 0 \tag{4}$$

The equilibrium equations satisfied by the stresses, the strain-displacement relations, and the electric field-potential relations are given by

$$T_{ij,j} = 0 \tag{5}$$

$$S_{ij} = (u_{i,j} + u_{j,i})/2 \tag{6}$$

$$E_i = -\varphi_{,i} \tag{7}$$

where  $u_i$  is the displacement vector and  $\varphi$  is the electric potential.

We assume that the TE and PE layers are perfectly bonded mechanically and the two layers are in local thermal equilibrium. That is, the TE and PE layers have the same displacement and temperature distributions in the in-plane directions. Moreover, the two layers are assumed to be shielded and insulated electrically. That is, the electric fields in the two layers will not interfere with each other. This may be achieved by coating the PE layer with a nanoscale electrically insulating and shielding flexible film [17]. The out-of-plane stresses can be neglected because the thickness of the bilayer structure is much smaller than its length  $L$ . The normal strain in the width direction can also be ignored if the width is much larger than the length  $L$ . The TE-PE problem thus can be treated as a one-dimensional (1D) problem with heat and current flowing in the  $z$ -, i.e.,  $x_3$ -direction. In this paper, we use a 1D strength of materials model to investigate the thermomechanical responses of the TE-PE bilayer structure. The 1D models may be used to determine the temperature, thermal stress, and deformation in the preliminary design of microelectronic structures [2,10–13]. Bending can occur in the bilayer structure due to the difference in the thermal expansion between the PE and TE layers. The effect of bending on the deformation is secondary and may be ignored when the thermal expansion difference in the TE leg direction is small, which is the case in this study. Now, the constitutive equations in Equation (1) for the TE layer reduce to

$$J_3 = \sigma E_3^{(1)} - \sigma S \frac{d\Theta}{dz} \tag{8}$$

$$h_3^{(1)} = -k^{(1)} \frac{d\Theta}{dz} + S\Theta J_3 \tag{9}$$

$$T_{33}^{(1)} = \frac{2G}{1-\nu} S_{33} - \frac{2G(1+\nu)\alpha^{(1)}}{1-\nu} (\Theta - \Theta_c) \tag{10}$$

where the superscript (1) denotes the quantities in the TE layer. The charge balance in Equation (3) under the 1D conditions means that the current density  $J_3$  is a constant in the TE film.

The constitutive equations for the PE layer reduce to

$$h_3^{(2)} = -k_3^{(2)} \frac{d\Theta}{dz} \tag{11}$$

$$T_{33}^{(2)} = c'_{33} S_{33} - e'_{33} E_3^{(2)} - \lambda_3'^{(2)} (\Theta - \Theta_c) \tag{12}$$

$$D_3^{(2)} = e'_{33} S_{33} + \epsilon'_{33} E_3^{(2)} + p'_3 (\Theta - \Theta_c) \tag{13}$$

where the superscript (2) stands for the quantities in the PE layer, and the primed constants are the effective properties given by

$$\begin{aligned} c'_{33} &= -c_{31}^{(2)} \frac{c_{13}^{(2)}}{c_{11}^{(2)}} + c_{33}^{(2)} \\ e'_{33} &= -c_{31}^{(2)} \frac{e_{31}^{(2)}}{c_{11}^{(2)}} + e_{33} \end{aligned} \tag{14}$$

$$\begin{aligned} \epsilon'_{33} &= e_{31} \frac{e_{31}^{(2)}}{c_{11}^{(2)}} + \epsilon_{33} \\ \lambda_3'^{(2)} &= -c_{31}^{(2)} \frac{\lambda_1^{(2)}}{c_{11}^{(2)}} + \lambda_3^{(2)} \end{aligned} \tag{15}$$

$$p'_3 = e_{31} \frac{\lambda_1^{(2)}}{c_{11}^{(2)}} + p_3$$

$$\begin{aligned} \lambda_3^{(2)} &= c_{13}^{(2)} \alpha_1^{(2)} + c_{23}^{(2)} \alpha_2^{(2)} + c_{33}^{(2)} \alpha_3^{(2)} \\ \lambda_1^{(2)} &= c_{11}^{(2)} \alpha_1^{(2)} + c_{12}^{(2)} \alpha_2^{(2)} + c_{13}^{(2)} \alpha_3^{(2)} \end{aligned} \tag{16}$$

In Equation (16),  $\alpha_i^{(2)}$  ( $i = 1, 2, 3$ ) are the coefficients of thermal expansion of the PE layer. The charge equation in Equation (4) under the 1D conditions means that the electric displacement  $D_3^{(2)}$  is a constant in the PE layer.

In general, the properties TE and PE materials are dependent on temperature. In this work, we conduct a first-order approximation investigation and assume that the material parameters are constant as in the studies of the classical work of thermoelectrics [18]. The assumption is reasonable considering the small temperature differential between the cold and hot ends of the TE film.

We use the following boundary conditions for the temperature field:

$$\begin{aligned} \Theta &= \Theta_c, z = 0 \\ \Theta &= \Theta_h, z = L \end{aligned} \tag{17}$$

We also assume no surface charge concentration at the two ends of the PE layer. The boundary conditions for the electric displacement can thus be written as

$$D_3^{(2)} = 0, z = 0, L \tag{18}$$

Finally, we consider fixed-end mechanical boundary conditions described by

$$u_3 = 0, z = 0, L \tag{19}$$

### 3. Temperature, Displacement, and Strain

The governing equations for the temperature and displacement in the hybrid bilayer structure can be derived by considering energy balance and force equilibrium of a differen-

tial element of the layered structure in the longitudinal direction (i.e., the z-direction). The energy balance gives

$$t_1 \frac{dh^{(1)}}{dz} + t_2 \frac{dh^{(2)}}{dz} + 2\eta(\Theta - \Theta_c) = t_1 J E_3^{(1)} \tag{20}$$

where  $\eta$  is the heat transfer coefficient at the two surfaces of the bilayer, and  $J = J_3$  is the constant current density in the TE leg. Using Equations (8), (9) and (11) in the above equation yields

$$\tilde{k} \frac{d^2(\Theta - \Theta_c)}{dz^2} - \frac{2\eta}{t_1}(\Theta - \Theta_c) = -\rho J^2 \tag{21}$$

where  $\rho = 1/\sigma$  is the electrical resistivity of the TE film, and  $\tilde{k}$  is an effective thermal conductivity given by

$$\tilde{k} = k^{(1)} + k_3^{(2)} \frac{t_2}{t_1} \tag{22}$$

The force balance of a longitudinal differential element leads to

$$\frac{dT_{33}^{(1)}}{dz} t_1 + \frac{dT_{33}^{(2)}}{dz} t_2 = 0 \tag{23}$$

The electric displacement in the PE layer is zero considering that  $D_3^{(2)}$  is a constant and it satisfies the homogeneous boundary condition (18). Equation (13) now becomes

$$e'_{33} S_{33} + \epsilon'_{33} E_3^{(2)} + p'_3(\Theta - \Theta_c) = 0 \tag{24}$$

Using Equations (10), (12) and (24) in Equation (23) yields

$$\tilde{c}_{33} \frac{d^2 u_3}{dz^2} - \tilde{\lambda}_{33} \frac{d\Theta}{dz} = 0 \tag{25}$$

where the effective properties are given by

$$\begin{aligned} \tilde{c}_{33} &= \frac{2G}{1-\nu} \frac{t_1}{t_2} + c'_{33} + e'_{33} \frac{e'_{33}}{\epsilon'_{33}} \\ \tilde{\lambda}_{33} &= \frac{2G(1+\nu)\alpha}{1-\nu} \frac{t_1}{t_2} + \lambda'_{33} - e'_{33} \frac{p'_3}{\epsilon'_{33}} \end{aligned} \tag{26}$$

The temperature distribution that satisfies Equation (21) and the boundary conditions in Equation (17) can be obtained as follows

$$\Theta = \Theta_c + A \exp(\lambda z) + B \exp(-\lambda z) + \frac{t_1}{2\eta} \rho J^2 \tag{27}$$

where  $\lambda$  is a parameter given by

$$\lambda = \sqrt{\frac{2\eta}{\tilde{k}t_1}} \tag{28}$$

and  $A$  and  $B$  are constants given by

$$\begin{aligned} A &= \frac{1}{\exp(\lambda L) - \exp(-\lambda L)} \left\{ \Delta\Theta - [1 - \exp(-\lambda L)] \frac{t_1}{2\eta} \rho J^2 \right\} \\ B &= \frac{1}{\exp(\lambda L) - \exp(-\lambda L)} \left\{ -\Delta\Theta - [\exp(\lambda L) - 1] \frac{t_1}{2\eta} \rho J^2 \right\} \end{aligned} \tag{29}$$

in which  $\Delta\Theta = \Theta_h - \Theta_c$  is the temperature differential between the hot and cold ends of the TE film.

The displacement in the laminate can be obtained by solving Equation (25) under the boundary conditions in Equation (19) as follows

$$u_3 = \frac{\tilde{\lambda}_{33}}{\tilde{c}_{33}} \left( \frac{A}{\lambda} e^{\lambda z} - \frac{B}{\lambda} e^{-\lambda z} + \frac{t_1}{2\eta} \rho J^2 z + C_1 z + C_2 \right) \tag{30}$$

where

$$\begin{aligned} C_1 &= -\frac{A}{\lambda L} e^{\lambda L} + \frac{B}{\lambda L} e^{-\lambda L} - \frac{t_1}{2\eta} \rho J^2 - \frac{B-A}{\lambda L} \\ C_2 &= \frac{B-A}{\lambda} \end{aligned} \tag{31}$$

The strain is then obtained as

$$S_{33} = \frac{du_3}{dz} = \frac{\tilde{\lambda}_{33}}{\tilde{c}_{33}} \left( A e^{\lambda z} + B e^{-\lambda z} + \frac{t_1}{2\eta} \rho J^2 + C_1 \right) \tag{32}$$

#### 4. Electric Fields and Stresses

The electric displacement in the PE layer is zero considering that  $D_3$  is a constant and it satisfies the homogeneous boundary condition (18). The electric field in the PE layer is thus obtained from Equations (24), (27) and (32) as follows

$$\begin{aligned} E_3^{(2)} &= -\frac{e'_{33} \tilde{\lambda}_{33}}{\epsilon'_{33} \tilde{c}_{33}} \left( A e^{\lambda z} + B e^{-\lambda z} + \frac{t_1}{2\eta} \rho J^2 + C_1 \right) \\ &\quad - \frac{p'_3}{\epsilon'_{33}} \left[ A \exp(\lambda z) + B \exp(-\lambda z) + \frac{t_1}{2\eta} \rho J^2 \right] \end{aligned} \tag{33}$$

Substituting Equation (33) into Equation (12) yields the stress in the PE layer

$$\begin{aligned} T_{33}^{(2)} &= \left( c'_{33} + e'_{33} \frac{e'_{33}}{\epsilon'_{33}} \right) \frac{\tilde{\lambda}_{33}}{\tilde{c}_{33}} \left( A e^{\lambda z} + B e^{-\lambda z} + \frac{t_1}{2\eta} \rho J^2 + C_1 \right) \\ &\quad - \left( \lambda'_3 - e'_{33} \frac{p'_3}{\epsilon'_{33}} \right) \left[ A \exp(\lambda z) + B \exp(-\lambda z) + \frac{t_1}{2\eta} \rho J^2 \right] \end{aligned} \tag{34}$$

The electric field in the TE layer is obtained from Equations (8) and (27) as follows

$$E_3^{(1)} = \rho J + S\lambda [A \exp(\lambda z) - B \exp(-\lambda z)] \tag{35}$$

Finally, the stress in the TE layer can be obtained from Equations (10), (27) and (32) as follows

$$\begin{aligned} T_{33}^{(1)} &= \frac{2G}{1-\nu} \frac{\tilde{\lambda}_{33}}{\tilde{c}_{33}} \left( A e^{\lambda z} + B e^{-\lambda z} + \frac{t_1}{2\eta} \rho J^2 + C_1 \right) \\ &\quad - \frac{2G(1+\nu)\alpha^{(1)}}{1-\nu} \left[ A \exp(\lambda z) + B \exp(-\lambda z) + \frac{t_1}{2\eta} \rho J^2 \right] \end{aligned} \tag{36}$$

#### 5. Thermoelectric Energy Conversion Efficiency

The energy conversion efficiency of the TE film is calculated by

$$\eta = \frac{t_1}{h_3^{(1)}(L)t_1 + h_3^{(2)}(L)t_2} \int_0^L J E_3^{(1)} dz \tag{37}$$

where

$$\int_0^L J E_3^{(1)} dz = \rho J^2 L + JS(\Theta_h - \Theta_c) \tag{38}$$

and

$$h_3^{(1)}(L) = -k^{(1)}\lambda[A \exp(\lambda L) - B \exp(-\lambda L)] + JS \left[ \Theta_c + A \exp(\lambda L) + B \exp(-\lambda L) + \frac{t_1}{2\eta} \rho J^2 \right] \tag{39}$$

$$h_3^{(2)}(L) = -k_3^{(2)}\lambda[A \exp(\lambda L) - B \exp(-\lambda L)] \tag{40}$$

### 6. Numerical Results and Discussion

In the numerical calculations, the TE material is a Bi<sub>2</sub>Te<sub>3</sub> with the properties listed in Table 1. The thermoelectric properties are taken from Lan et al. [19]. The elastic modulus and coefficient of thermal expansion are from Tsai et al. [20] and Chen et al. [21], respectively. The piezoelectric material is PZT-5H with the properties listed in Table 2 [22–24]. The temperatures at the cold and hot ends of the hybrid structure are  $\Theta_c = 290$  K and  $\Theta_h = 330$  K, respectively. The composite length is assumed to be  $L = 500$   $\mu\text{m}$  and the TE layer has a thickness of 5  $\mu\text{m}$  in the numerical examples. The heat transfer coefficient at the two surfaces of the bilayer is assumed as  $\eta = 20$  W/(m<sup>2</sup>K).

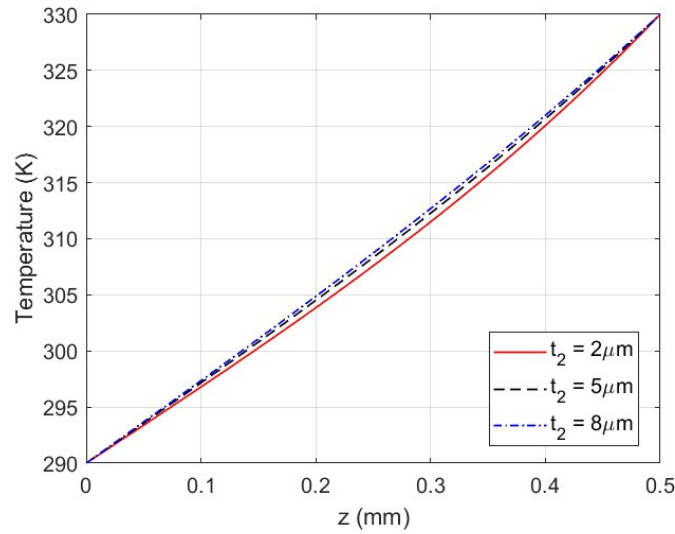
**Table 1.** Material properties of the TE layer.

|   |                              |
|---|------------------------------|
| Young’s modulus (GPa)   | $E = 110$                    |
| Poisson’s ratio   | $\nu = 0.30$                 |
| Coefficient of thermal expansion<br>( $10^{-6}$ K <sup>-1</sup> ) | $\alpha = 15$                |
| Thermal conductivity (W/(m-K))                                    | $k = 1.2$                    |
| Electrical resistivity ( $\Omega\text{-m}$ )                      | $\rho = 0.82 \times 10^{-5}$ |
| Seebeck coefficient ( $\mu\text{V/K}$ )                           | $S = 191$                    |

**Table 2.** Material properties of the PZT-5H layer.

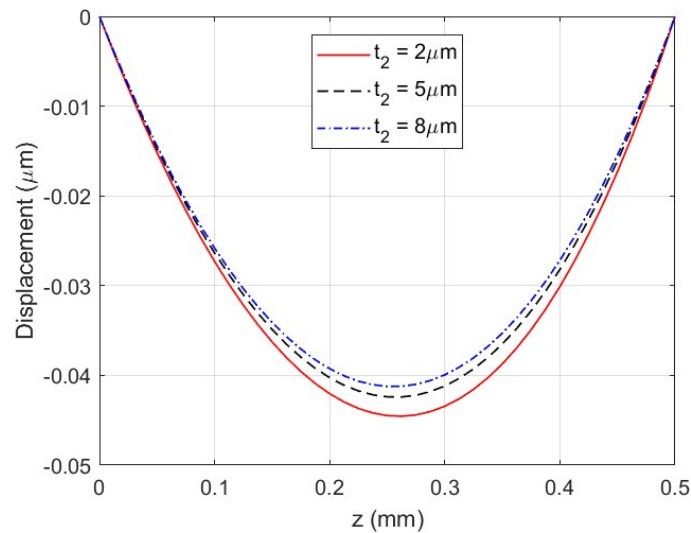
|   |  |
|---|--|
| Elastic constants (GPa)   | $c_{33} = 117, c_{31} = c_{32} = 84.1,$<br>$c_{11} = 126, c_{12} = 79.5$ |
| Piezoelectric constants (C/m <sup>2</sup> )                       | $e_{33} = 23.3, e_{31} = -6.5$   |
| Dielectric constant (V-m)   | $\epsilon_{33} = 1470\epsilon_0 = 1.302 \times 10^{-8}$                  |
| Coefficient of thermal expansion<br>( $10^{-6}$ K <sup>-1</sup> ) | $\alpha_1 = -3.3$<br>$\alpha_2 = -3.3$<br>$\alpha_3 = 15.8$              |
| Thermal conductivity (W/(m-K))                                    | $k_3 = 1.5$  |
| Pyroelectric constant (C/(m <sup>2</sup> -K))                     | $p_3 = -400 \times 10^{-6}$  |

Figure 2 shows the temperature distribution in the bilayer structure for various values of the PE layer thickness. In all cases, the temperature increases from the prescribed cold side temperature of 290 K to the prescribed hot side temperature of 330 K. At a given axial location, the temperature slightly increases with an increase in the PE layer thickness; that is, the temperature is higher when the PE thickness is larger than the TE layer thickness ( $t_2/t_1 = 1.6$ ), whereas the temperature is lower when the PE layer is thinner than the TE layer ( $t_2/t_1 = 0.4$ ). This is because the PE layer has a slightly higher thermal conductivity than the TE layer and hence the overall heat flux in the bilayer structure becomes higher with a thicker PE layer.



**Figure 2.** Temperature distribution in the TE-PE bilayer ( $t_1 = 5 \mu\text{m}$ ).

Figure 3 shows the displacement distribution in the bilayer structure for various values of the PE layer thickness. The displacement field slightly deviates from the symmetric distribution about the midpoint of the structure. The negative displacement means that the material points move towards the cold end ( $z = 0$ ) of the structure. i.e., from the higher temperature region to the lower temperature region. The magnitude of the displacement gradually increases towards the mid portion of the film. The maximum magnitude of the displacement of  $0.04455 \mu\text{m}$  occurs at  $z = 0.263 \text{ mm}$  for  $t_2/t_1 = 0.4$ . The magnitude of the displacement increases with a decrease in the PE layer thickness as well as in the overall bilayer thickness because the TE layer thickness is fixed. The characteristics of the displacement distribution will be further elaborated in the discussion of the strain distribution.



**Figure 3.** Displacement distribution in the TE-PE bilayer ( $t_1 = 5 \mu\text{m}$ ).

Figure 4 shows the strain distribution in the bilayer structure for various values of the PE layer thickness. The strain is compressive in the cold-side region ( $z < 0.263 \text{ mm}$ ) and becomes tensile in the hot-side region ( $z > 0.263 \text{ mm}$ ). The magnitude of the strain at the hot end  $z = L$  is larger than that at the cold end  $z = 0$ . These strain distribution characteristics are due to the fact that the temperature in the hot side of the bilayer is higher than the reference temperature (the same as the cold-end temperature as assumed), which causes expansion and therefore positive strain in the region. In the meantime, the integral of the strain over the bilayer length equals zero (fixed ends) and hence the strain in the cold-side region must

be negative. The above also explains why the displacement is in the negative z-direction. The larger strain at the hot end is mostly the result of the difference between the hot-end temperature and the reference temperature. At a given axial location, the magnitude of the strain increases with a decrease in the PE layer thickness, which is a result of lower overall stiffness of the bilayer structure with a thinner PE layer.

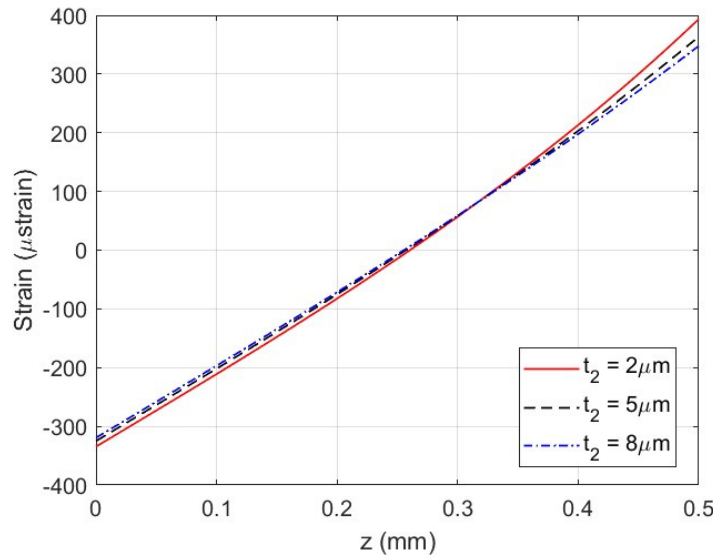


Figure 4. Strain distribution in the TE-PE bilayer ( $t_1 = 5 \mu\text{m}$ ).

Figure 5 shows the stress distribution in the PE layer for various values of the PE layer thickness. The magnitude of the compressive stress increases with increasing distance from the hot end  $z = L$ . For  $t_2 = t_1 = 5 \mu\text{m}$ , the magnitude of the stress at the hot end  $z = L$  is 27.35 MPa and increases to 38.39 MPa at the cold end  $z = 0$ . It is seen that with a decrease in the PE layer thickness, the magnitude of the compressive stress increases near the cold end  $z = 0$ , but decreases in the hot-side region. As indicated by Equation (12), the stress depends on the strain, the electric field, and the temperature variation from the reference value. The higher tensile strain in the hot-side region and the lower electric field intensity (as shown in the following Figure 6) may contribute to the lower magnitude of the compressive stress near the hot end of the bilayer structure with a thinner PE layer.

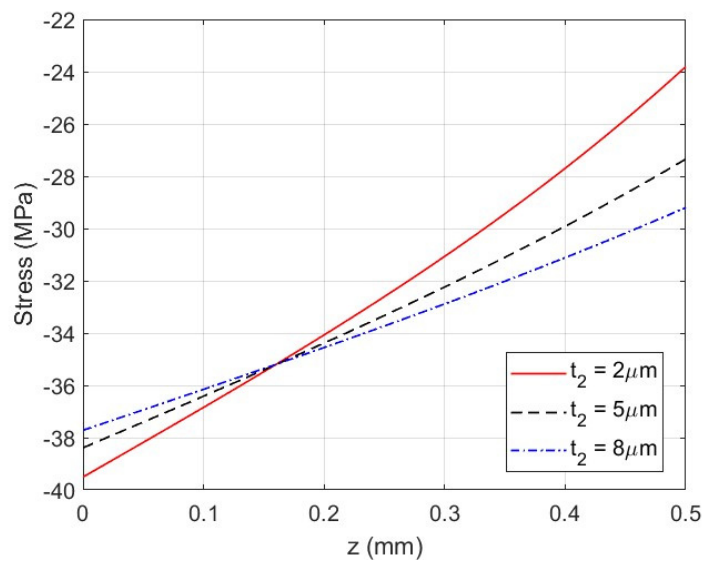
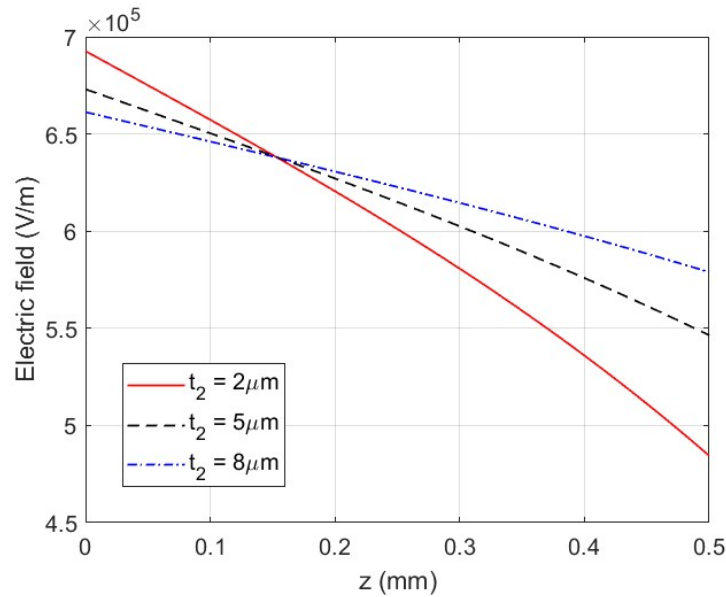


Figure 5. Stress distribution in the PE layer ( $t_1 = 5 \mu\text{m}$ ).



**Figure 6.** Electric field in the PE layer ( $t_1 = 5 \mu\text{m}$ ).

Figure 6 shows the electric field in the PE layer for various values of the PE layer thickness. For a given PE thickness, the electric field intensity decreases from the maximum value at the cold end ( $z = 0$ ) with increasing distance from the cold end. At a given location, a lower PE thickness results in a higher electric field near the cold end and lower electric field in the hot-side region. Corresponding to the electric field, the electrical potential difference between the two ends of the PE membrane are 298, 307, and 311 V for  $t_2 = 2, 5,$  and  $8 \mu\text{m}$ , respectively.

Figure 7 shows the stress distribution in the TE layer for various values of the PE layer thickness. As indicated by Equation (10), the stress in the TE layer depends on the strain and the temperature variation from the reference value. Different from the stress distribution in the PE layer as shown in Figure 5, now the magnitude of the compressive stress decreases with increasing distance from the hot end  $z = L$ , reflecting the absence of the influence of the electric field on the stress. For  $t_2 = t_1 = 5 \mu\text{m}$ , the magnitude of the stress at the hot end  $z = L$  is 50.34 MPa and decreases to 39.3 MPa at the cold end  $z = 0$ .

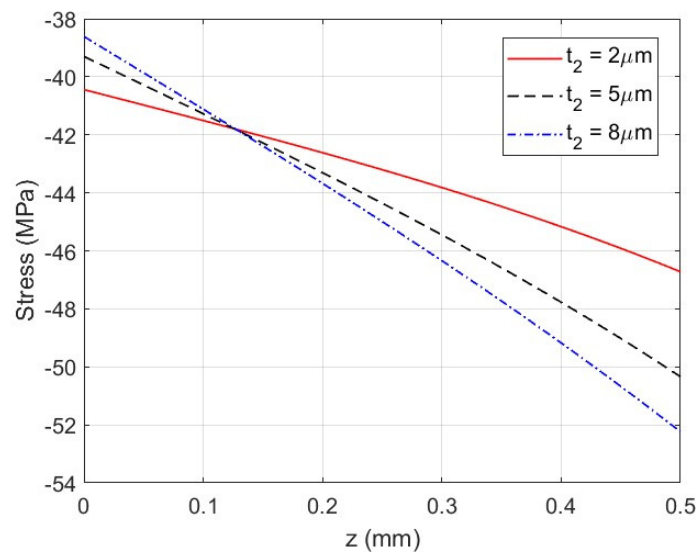


**Figure 7.** Stress distribution in the TE layer ( $t_1 = 5 \mu\text{m}$ ).

Figures 5 and 7 show that the extreme stresses occur at the ends of the TE-PE structure. Figure 8 shows the stresses at the cold end  $z = 0$  and the hot end  $z = L$  in both the TE and PE layers as functions of the PE layer thickness. It is seen that the stresses at the two ends of the TE layer become almost the same while the stresses at the two ends of the PE layer deviate when the PE layer thickness becomes vanishingly small. The convergence of the stresses at the two ends in the TE layer indicates that the stress becomes uniform in the TE layer, which is expected because mechanically the force in the structure is basically supported by the TE layer when the PE layer thickness is extremely small. With decreasing PE layer thickness, the maximum magnitude of the stress in the PE layer increases whereas the maximum stress in the TE layer decreases. The maximum magnitude of the compressive stress in the PZT-5H layer is generally below the strength of the material [25]. However, the magnitude of the compressive stress in the  $\text{Bi}_2\text{Te}_3$  layer may become higher than the material strength. For example, Keshavarz et al. [26] reported the strength values between 62 MPa and 120 MPa for  $\text{Bi}_2\text{Te}_3$  under different processing conditions. Qian et al. [27] reported the strength values between 24 MPa and 67 MPa for  $\text{Bi}_2\text{Te}_3$ -based alloys. The model developed in this work may be used to determine the thicknesses and the temperature differentials under which mechanical failure may occur.

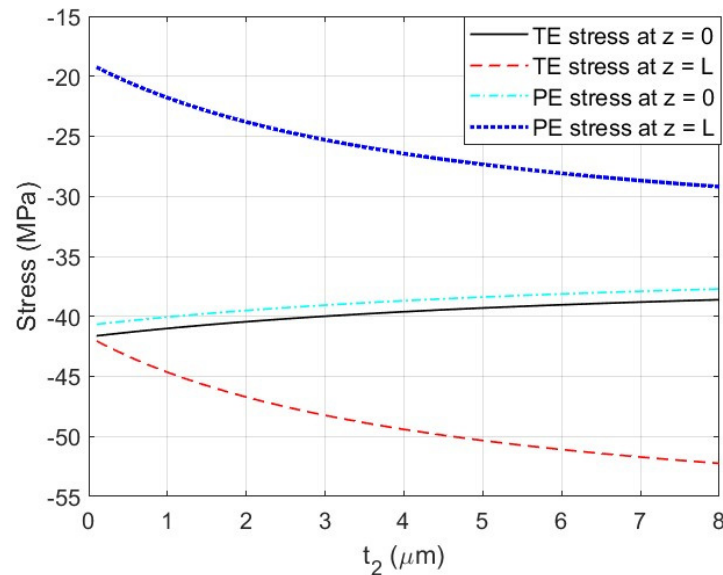
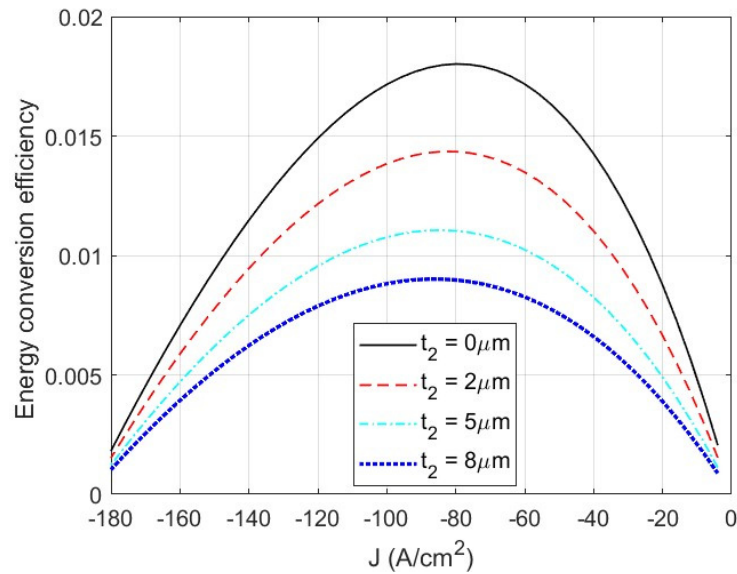


Figure 8. Stress distribution in the TE layer ( $t_1 = 5 \mu\text{m}$ ).

Figure 9 shows the effect of the PE layer thickness on the energy conversion efficiency of the bilayer TE-PE structure, where  $t_2 = 0$  means the efficiency of a single TE leg without the PE support/sensing layer. It is clear that the efficiency decreases with an increase in the PE layer thickness. This is because a portion of the thermal energy at the hot end is used to heat the PE layer instead of being used to generate electricity in the TE layer. The decrease in the energy conversion efficiency is significant as the peak efficiency decreases from 0.018 for the stand-alone TE layer to 0.0111 for the TE-PE bilayer with the same TE and PE thickness ( $t_1 = t_2 = 0.5 \mu\text{m}$ ). In general, the TE energy efficiency decreases monotonically with increasing PE layer thickness.



**Figure 9.** Energy conversion efficiency of the TE-PE bilayer structure ( $t_1 = 5 \mu\text{m}$ ).

## 7. Conclusions

In this paper, we propose to use a piezoelectric layer as both a support membrane and a sensor for a thermoelectric film for microelectronics applications. We analyze a hybrid TE-PE bilayer structure with the two layers being perfectly bonded mechanically and in local thermal equilibrium. The two layers are electrically shielded and insulated with each other. The temperature, displacement, and strain fields in the bilayer and the stresses in both the PE and TE layers are obtained. The effect of the PE layer on the TE energy conversion efficiency is examined.

Our numerical results for a  $\text{Bi}_2\text{Te}_3/\text{PZT-5H}$  bilayer show that with an increase in the PE layer thickness, the temperature in the hybrid bilayer slightly increases. In the meantime, the magnitudes of the displacement and strain decrease. With decreasing PE layer thickness, the magnitudes of the compressive stresses in the both PE and TE layers increase at the cold end  $z = 0$  but decrease at the hot end  $z = L$ . The largest compressive stress in the PE layer occurs at the cold end. In the TE layer, however, the largest compressive stress occurs at the hot end. The maximum compressive stress in the PZT-5H layer is generally below the strength of the material for the geometrical parameters considered in this paper. However, the maximum compressive stress in the  $\text{Bi}_2\text{Te}_3$  layer may reach the material strength depending on the material processing conditions. The model developed in this work may be used to determine the thicknesses and the temperature differentials under which failure may occur. Buckling of thin TE-PE structures is another possible failure mode under large compressive stresses. Jin [28] showed that buckling of TE films and laminated TE film/regular support membranes may occur for large TE leg length/thickness ratios. Buckling of hybrid TE-PE structures and the piezoelectric effects will be addressed in future investigations.

The numerical results show that the thermoelectric energy conversion efficiency is negatively influenced by the PE supporting/sensing layer. The decrease in the energy efficiency can be significant as a nearly 40% reduction in the peak efficiency occurs for a TE-PE structure with a PE layer of the same thickness as that of the TE layer. In general, the TE energy efficiency decreases monotonically with increasing PE layer thickness. Hence, thin PE layers should be used to improve the energy efficiency. Moreover, thin PE layers also reduce the compressive stress in the TE layer. However, buckling will become an issue for extremely thin TE-PE structures. In general, design of TE films with supporting/sensing membranes must consider both aspects of thermomechanical reliability and energy conversion efficiency.

**Author Contributions:** Conceptualization, Z.J. and J.Y.; methodology, Z.J. and J.Y.; software, Z.J.; validation, Z.J. and J.Y.; formal analysis, Z.J. and J.Y.; investigation, Z.J. and J.Y.; resources, Z.J. and J.Y.; data curation, Z.J. and J.Y.; writing—original draft preparation, Z.J.; writing—review and editing, Z.J. and J.Y.; visualization, Z.J. and J.Y.; supervision, Z.J. and J.Y.; project administration, Z.J. and J.Y.; funding acquisition, Z.J. and J.Y. All authors have read and agreed to the published version of the manuscript.

**Funding:** This research received no external funding.

**Data Availability Statement:** Data is contained within the article.

**Acknowledgments:** The authors would like to thank three anonymous reviewers for their helpful comments on improving upon the presentation of this work.

**Conflicts of Interest:** The authors declare no conflict of interest.

## References

- Rowe, D.M.; Morgan, D.V.; Keily, J.H. Miniature low-power/high-voltage thermoelectric generator. *Electron. Lett.* **1989**, *25*, 166–168. [[CrossRef](#)]
- Volklein, F.; Min, G.; Rowe, D.M. Modeling of a microelectromechanical thermoelectric cooler. *Sens. Actuators A* **1999**, *75*, 95–101. [[CrossRef](#)]
- Venkatasubramanian, R.; Siivola, E.; Colpitts, T.; O’Quinn, B. Thin-film thermoelectric devices with high room-temperature figures of merit. *Nature* **2001**, *413*, 597–602. [[CrossRef](#)] [[PubMed](#)]
- Chen, G.; Dresselhaus, M.S.; Dresselhaus, G.; Fleurial, J.P.; Caillat, T. Recent development in thermoelectric materials. *Int. Mater. Rev.* **2003**, *48*, 45–66. [[CrossRef](#)]
- Kogo, G.; Xiao, B.; Danquah, S.; Lee, H.; Niyogushima, J.; Yarbrough, K.; Candadai, A.; Marconnet, A.; Pradhan, S.; Bahoura, M. A thin film efficient pn-junction thermoelectric device fabricated by self-align shadow mask. *Sci. Rep.* **2020**, *10*, 1067. [[CrossRef](#)] [[PubMed](#)]
- Corbett, S.; Gautam, D.; Lal, S.; Yu, K.; Balla, N.; Cunningham, G.; Razeeb, K.M.; Enright, R.; McCloskey, D. Electrodeposited thin-film micro-thermoelectric coolers with extreme heat Flux handling and microsecond time response. *ACS Appl. Mater. Interfaces* **2021**, *13*, 1773–1782. [[CrossRef](#)] [[PubMed](#)]
- Nandihalli, N. A short account of thermoelectric film characterization techniques. *Mater. Today Phys.* **2023**, *36*, 101173. [[CrossRef](#)]
- Mele, P.; Narducci, D.; Ohta, M.; Biswas, K.; Morante, J.; Saini, S.; Endo, T. (Eds.) *Thermoelectric Thin Films*; Springer: Cham, Switzerland, 2019.
- Kong, D.; Zhu, W.; Guo, Z.; Deng, Y. High-performance flexible Bi<sub>2</sub>Te<sub>3</sub> films based wearable thermoelectric generator for energy harvesting. *Energy* **2019**, *175*, 292–299. [[CrossRef](#)]
- Huang, M.J.; Chou, P.K.; Lin, M.C. Thermal and thermal stresses of a thin-film thermoelectric cooler under the influence of the Thomson effect. *Sens. Actuators A* **2006**, *126*, 122–128. [[CrossRef](#)]
- Huang, M.J.; Chou, P.K.; Lin, M.C. An Investigation of the thermal stresses induced in a thin-film thermoelectric cooler. *J. Therm. Stress.* **2008**, *31*, 438–454. [[CrossRef](#)]
- Jin, Z.H. Thermal stresses in a multilayered thin film thermoelectric structure. *Microelectron. Reliab.* **2014**, *54*, 1363–1368. [[CrossRef](#)]
- Jin, Z.H.; Yang, J.S. Analysis of a sandwiched piezoelectric semiconducting thermoelectric structure. *Mech. Res. Commun.* **2019**, *98*, 31–36. [[CrossRef](#)]
- Giurgiutiu, V. *Structural Health Monitoring with Piezoelectric Wafer Active Sensors*, 2nd ed.; Academic Press: New York, NY, USA, 2014.
- Güemes, A.; Fernandez-Lopez, A.; Pozo, A.R.; Sierra-Pérez, J. Structural Health Monitoring for Advanced Composite Structures: A Review. *J. Compos. Sci.* **2020**, *4*, 13. [[CrossRef](#)]
- Ghadarah, N.; Ayre, D. A Review on acoustic emission testing for structural health monitoring of polymer-based composites. *Sensors* **2023**, *23*, 6945. [[CrossRef](#)] [[PubMed](#)]
- Barani, Z.; Kargar, F.; Ghafouri, Y.; Ghosh, S.; Godziszewski, K.; Baraghani, S.; Yashchyshyn, Y.; Cywiński, G.; Rummyantsev, S.; Salguero, T.T.; et al. Electrically insulating flexible films with quasi-1D van der Waals fillers as efficient electromagnetic shields in the GHz and Sub-THz frequency bands. *Adv. Mater.* **2021**, *33*, 2007286. [[CrossRef](#)] [[PubMed](#)]
- Rowe, D.M. (Ed.) *CRC Handbook of Thermoelectrics*; CRC Press: Boca Raton, FL, USA, 1995.
- Lan, Y.; Minnich, A.J.; Chen, G.; Ren, Z. Enhancement of thermoelectric figure-of-merit by a bulk nanostructuring approach. *Adv. Funct. Mater.* **2010**, *20*, 357–376. [[CrossRef](#)]
- Tasi, C.-H.; Tseng, Y.-C.; Jian, S.R.; Liao, Y.-Y.; Lin, C.-M.; Yang, P.-F.; Chen, D.-L.; Chen, H.-J.; Luo, C.-W.; Juang, J.-Y. Nanomechanical properties of Bi<sub>2</sub>Te<sub>3</sub> thin films by nanoindentation. *J. Alloys Compd.* **2015**, *619*, 834–838. [[CrossRef](#)]
- Chen, X.; Zhou, H.D.; Kiswandhi, A.; Miotkowski, I.; Chen, Y.P.; Sharma, P.A.; Lima Sharma, A.L.; Hekmaty, M.A.; Smirnov, D.; Jiang, Z. Thermal expansion coefficients of Bi<sub>2</sub>Se<sub>3</sub> and Sb<sub>2</sub>Te<sub>3</sub> crystals from 10 K to 270 K. *Appl. Phys. Lett.* **2011**, *99*, 261912. [[CrossRef](#)]
- Yang, J.S. *An Introduction to the Theory of Piezoelectricity*; Springer: New York, NY, USA, 2005.

23. Chang, H.H.S.; Huang, Z. Pyroelectric effect enhancement through product property under open circuit condition. *J. Appl. Phys.* **2009**, *106*, 014101. [[CrossRef](#)]
24. Zhang, Y.; Xie, M.; Roscow, J.; Bao, Y.; Zhou, K.; Zhang, D.; Bowen, C.R. Enhanced pyroelectric and piezoelectric properties of PZT with aligned porosity for energy harvesting applications. *J. Mater. Chem. A* **2017**, *5*, 6569–6580. [[CrossRef](#)] [[PubMed](#)]
25. Anton, S.R.; Erturk, A.; Inman, D. Bending strength of piezoelectric ceramics and single crystals for multifunctional load-bearing applications. *IEEE Trans. Ultrason. Ferroelectr. Freq. Control.* **2012**, *59*, 1085–1092. [[CrossRef](#)] [[PubMed](#)]
26. Keshavarz, M.K.; Vasilevskiy, D.; Masut, R.A.; Turenne, S. Mechanical properties of bismuth telluride based alloys with embedded MoS<sub>2</sub> nano-particles. *Mater. Des.* **2016**, *103*, 114–121. [[CrossRef](#)]
27. Qian, D.; Ye, Z.; Pan, L.; Zuo, Z.; Yang, D.; Yan, Y. The mechanical and thermoelectric properties of Bi<sub>2</sub>Te<sub>3</sub>-Bbased alloy prepared by constrained hot compression technique. *Metals* **2021**, *11*, 1060. [[CrossRef](#)]
28. Jin, Z.H. Buckling of thin film thermoelectrics. *Int. J. Fract.* **2013**, *180*, 129–136. [[CrossRef](#)]

**Disclaimer/Publisher’s Note:** The statements, opinions and data contained in all publications are solely those of the individual author(s) and contributor(s) and not of MDPI and/or the editor(s). MDPI and/or the editor(s) disclaim responsibility for any injury to people or property resulting from any ideas, methods, instructions or products referred to in the content.